Synthesis, Isolation, and Study of a Heterobimetallic Uranyl Crown-Ether Complex

Riddhi R. Golwankar,[a,#] Alexander C. Ervin,[a,#] Małgorzata Z. Makoś,[b] Emily R. Mikeska,[a] Vassiliki-Alexandra Glezakou,[b,] and James D. Blakemore[a,*]*

[a] Department of Chemistry, University of Kansas, 1567 Irving Hill Road, Lawrence, Kansas 66045, United States

[b] Chemical Sciences Division, Oak Ridge National Laboratory, Oak Ridge, Tennessee 37830, United States

[#]These authors contributed equally

* To whom correspondence should be addressed: blakemore@ku.edu (J.D.B.); glezakouva@ornl.gov (V.-A.G.)

Abstract: Although crown ethers can selectively bind many metal cations, little is known regarding the properties of crown ether complexes of the uranyl dication, UO_2^{2+}. Here, the synthesis and characterization of an isolable complex in which the uranyl dication is bound in an 18-crown-6-like moiety are reported. A tailored macrocyclic complex featuring an accessory Pt(II) center was used to drive capture of UO_2^{2+} by the crown, as demonstrated by results from single-crystal X-ray diffraction analysis. The U(V) oxidation state becomes accessible at a quite positive potential ($E_{1/2}$) of –0.18 V vs. $Fc^{+/0}$ upon complexation, representing the most positive U^{VI}/U^{V} potential yet reported for the UO_2^{n+} core moiety. Joint computational studies show that the electronic structure of the U(V) form results in significant weakening of U–O_{oxo} bonding despite the quite positive reduction potential at which this species can be accessed, underscoring that crown-ligated uranyl species could demonstrate unique reactivity under only modestly reducing conditions.

https://doi.org/10.26434/chemrxiv-2023-qb7cc **ORCID:** https://orcid.org/0000-0003-4172-7460 Content not peer-reviewed by ChemRxiv. **License:** CC BY-NC-ND 4.0

The ability of crown ethers to chelate alkali, alkaline earth, and transition metal ions has been extensively documented through both crystallography and chemical analysis.[1] From the perspectives of both coordination chemistry and supramolecular science, binding of metal cations in crown ether ligands has been demonstrated to impart unique and otherwise inaccessible properties to the resulting metal complexes, including modulated solubility, unique metal geometry, and modified speciation. In the area of radiochemistry,[2] crown ethers have been shown, in accord with the classic literature on the properties of crown ethers, to afford advantages in liquid-liquid extractions of products of fission.[3]

Conversely, few reports have described the binding/chelation of actinides in crown ethers, despite the ubiquity of these ligands and their usefulness for preparation of metal complexes. Most recently, 18-crown-6 complexes of Cf(III) and Am(III) were reported,[4] complementing older work on complexes featuring U(III)[5] and Pu(III)[6] encapsulated in 18-crown-6 ligands. Work has also demonstrated that the *trans*-dioxo actinyl-type species of U(VI),[7,8,9,10] Np(V),[11,12] and Pu(V)[13] can be chelated by 18-crown-6 derivatives in the solid state, leading to complexes featuring κ^6-crowns with outer-sphere counteranions. But, characterization of crown-coordinated actinide complexes wherein the actinide ion is threaded through the crown ether are rare; the majority of examples display actinide centers with water ligands in the first coordination sphere that hydrogen bond to crown ethers held in the secondary sphere.[14] Crown ethers and cryptands have also shown great utility in actinide organometallic chemistry; in these cases, crowns typical encapsulate countercations like Na^+ or K^+ that charge balance anionic actinide species.[15,16]

https://doi.org/10.26434/chemrxiv-2023-qb7cc **ORCID:** https://orcid.org/0000-0003-4172-7460 Content not peer-reviewed by ChemRxiv. **License:** CC BY-NC-ND 4.0

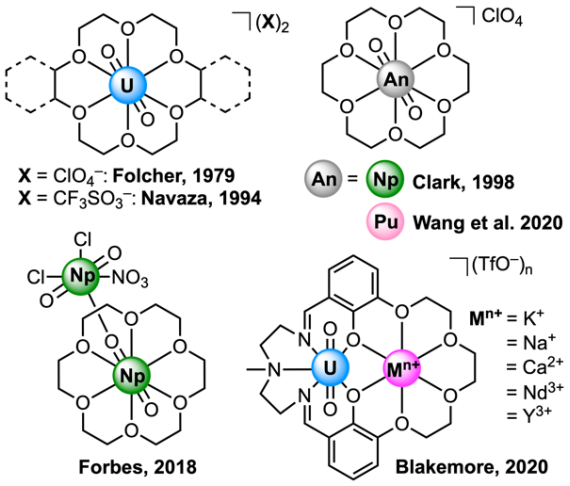

Scheme 1. Literature examples of crown ether complexes of actinyl ions.

Considering all of this prior work, we recently turned our attention toward the open questions of crown ether chelation of the U(VI) and U(V) oxidation states, as well as how such species might be interconverted in solution. As Ln(III) ions can undergo reduction to form less common Ln(II) analogues when ligated by crowns,[17] we anticipated that synthesis of crown-ether-ligated uranyl complexes could afford species with unique solution-phase redox and reactivity properties.

In order to generate isolable uranyl-crown complexes, we developed a specialized Pt(II)-containing macrocycle (denoted **1**) with a Reinhoudt-type ligand scaffold that presents an 18-crown-6-like site for binding of the uranyl ion, UO_2^{2+}. Such ligands have previously been used by our group to access related Ni(II),[18] Pd(II),[19] Zn(II),[20] and V(IV)[21] complexes, but here, a new method was developed for installation of a platinum center into the macrocycle (see Experimental Section in Supporting Information for details). We found that **1** could be prepared from the previously reported **[H$_2$,Ba]**[19] using $Ba(OH)_2$ as a base and $Pt(DMSO)_2Cl_2$ as a convenient metalating agent (see Scheme 2). With our procedure, **1** could be isolated as an orange powder in good yield (ca. 70%), and fully characterized by ^{1}H and ^{13}C{^{1}H} NMR, UV-visible absorption spectroscopy, and elemental analysis (see SI, pp. S6, S9-S11, and S18).

https://doi.org/10.26434/chemrxiv-2023-qb7cc **ORCID:** https://orcid.org/0000-0003-4172-7460 Content not peer-reviewed by ChemRxiv. **License:** CC BY-NC-ND 4.0

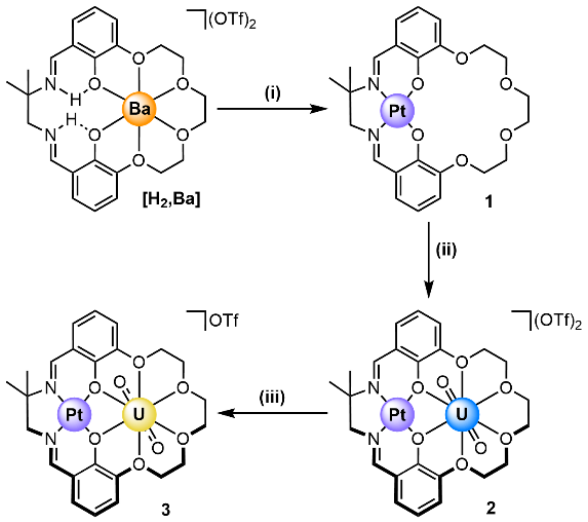

Scheme 2. Synthetic strategy for the preparation of **1**, **2**, and **3**. Conditions: (i) [a] 1.1 equiv. $Ba(OH)_2•8H_2O$, 0.95 equiv. $PtCl_2(DMSO)_2$, in DMF and approx. 5 mL DMSO, 60-65°C, 24 hours; [b] excess guanidinium sulfate in $CHCl_3$ and H_2O, 48 hours. (ii) 1 equiv. $UO_2(OTf)_2$ in CH_3CN, 30 minutes. (iii) [a] 1 equiv. Cp^*_2Fe in CH_3CN, 15 minutes; [b] 1 equiv. Cp_2Co in CH_3CN, 15 minutes. Complex **3** has either $Cp^*_2Fe^+(OTf)^-$ [conditions (iii) a] or $Cp_2Co^+(OTf)^-$ [conditions (iii) b] salts in the resulting product.

Single crystals of **1** suitable for X-ray diffraction (XRD) analysis were grown by vapor diffusion of hexanes into a dichloromethane (CH_2Cl_2) solution of the complex. In line with NMR spectral findings, the XRD structure of **1** (see Figure 1) confirmed the binding of Pt(II) in the salen-like [N_2,O_2] site of the ligand; a single co-crystallized water molecule was found interacting with the crown-ether-like site via H-bonding in the solid state, but we note that the complex can be fully dried, resulting in removal of water without any decomposition. Importantly, the platinum site is rigorously square planar (τ_4 = 0.04(1)) and thus assists with enforcing a high degree of flatness across the full macrocyclic structure. The planarity of the crown-ether-like site was quantified through the ω_{crown} parameter (see Table 1); the value of this parameter for **1** is 0.20(1), in accord with pre-arrangement of the six oxygen donors of the crown site and their readiness to bind UO_2^{2+}.

https://doi.org/10.26434/chemrxiv-2023-qb7cc **ORCID:** https://orcid.org/0000-0003-4172-7460 Content not peer-reviewed by ChemRxiv. **License:** CC BY-NC-ND 4.0

UO_2^{2+} was installed into the crown site by addition of 1 equiv. of anhydrous uranyl triflate, $UO_2(OTf)_2$, to **1** in CH_3CN. $UO_2(OTf)_2$ was prepared according to Ephritikhine's method,[22] with minor modifications as described in a prior report from our group.[23] Addition of $UO_2(OTf)_2$ to **1** resulted in an immediate change in the color of the solution from mango yellow to deep red; the resulting heterobimetallic uranyl crown complex (denoted **2**) could be isolated in virtually quantitative yield by filtration followed by removal of solvent *in vacuo*. ^1H, $^{13}C\{^1H\}$, and ^{19}F NMR spectra collected in CD_3CN confirmed the formation of **2** and its persistence in solution; a characteristic and significant downfield shift of the ^1H NMR resonances associated with the aliphatic protons of the ethylene bridges of the crown ether moiety was measured (from 3.6–4.1 ppm to 5.2–5.5 ppm), in line with threading of the uranyl ion into the crown. However, in line with the dicationic and highly Lewis acidic nature of UO_2^{2+}, downfield shifts were observed for all the other ^1H resonances associated with the ligand backbone of **2** in comparison to those for **1** (see Figure S17).

Chelation of UO_2^{2+} by the crown-ether oxygen atoms in **2** was confirmed by the single-crystal XRD structure of the heterobimetallic complex. Single crystals of **2** suitable for XRD analysis were grown by vapor diffusion of Et_2O into a CH_3CN solution of the complex. As anticipated from the NMR studies, the uranyl dication was found in the crown-ether-like site of the macrocyclic ligand, interacting with all six macrocyclic oxygen donor atoms. No additional solvent molecules or triflate counteranions bind to the U center; the triflate counteranions (2 per $[UO_2]$ unit) were found in the outer-sphere along with co-crystallized CH_3CN molecules presumably derived from the crystal growth conditions. The average $U–O_{oxo}$ bond distance was found to be 1.751(9) Å, in line with the U(VI) formal oxidation state[24] and the dicationic nature of the overall $[Pt,UO_2]^{2+}$ species. The average ω_{crown} parameter for **2** is 0.23(3), similar to the value of 0.20(1) found for **1**,

https://doi.org/10.26434/chemrxiv-2023-qb7cc **ORCID:** https://orcid.org/0000-0003-4172-7460 Content not peer-reviewed by ChemRxiv. **License:** CC BY-NC-ND 4.0

suggesting that little reorganization of the ligand is required for uranyl binding. In line with findings from prior work on crown systems from our group that examined binding of other cations, UO_2^{2+} nestles most closely toward the phenoxide O atoms that bridge to the Pt(II) center (see Figure S66) and sits most far away from O3/O6 in the crown-like site. The binding of UO_2^{2+} results in an overall contraction of the average O1•••O2 distance of the nascent heterobimetallic diamond core motif, from 2.74(5) Å in **1** to 2.59(2) Å in **2**; this is consistent with the Lewis acidic nature of UO_2^{2+} and interaction of both Pt^{2+} and UO_2^{2+} with the bridging atoms.

With **2** in hand, we moved to interrogate the redox properties of the complex in light of its unusual structure and the formally dicationic nature of the heterobimetallic [Pt,UO_2] core that we anticipated could lead to uncommon properties. As a preamble, we note that the electrochemical properties of the precursor **1** are unremarkable; cyclic voltammetry data show that this complex features single reduction event, likely ligand-centered in nature, [19,20] with a peak cathodic reduction potential ($E_{p,c}$) of –2.44 V vs. ferrocenium/ferrocene (denoted hereafter as $Fc^{+/0}$) in CH_3CN containing 0.1 M tetrabutylammonium hexafluorophosphate ($TBAPF_6$).

https://doi.org/10.26434/chemrxiv-2023-qb7cc **ORCID:** https://orcid.org/0000-0003-4172-7460 Content not peer-reviewed by ChemRxiv. **License:** CC BY-NC-ND 4.0

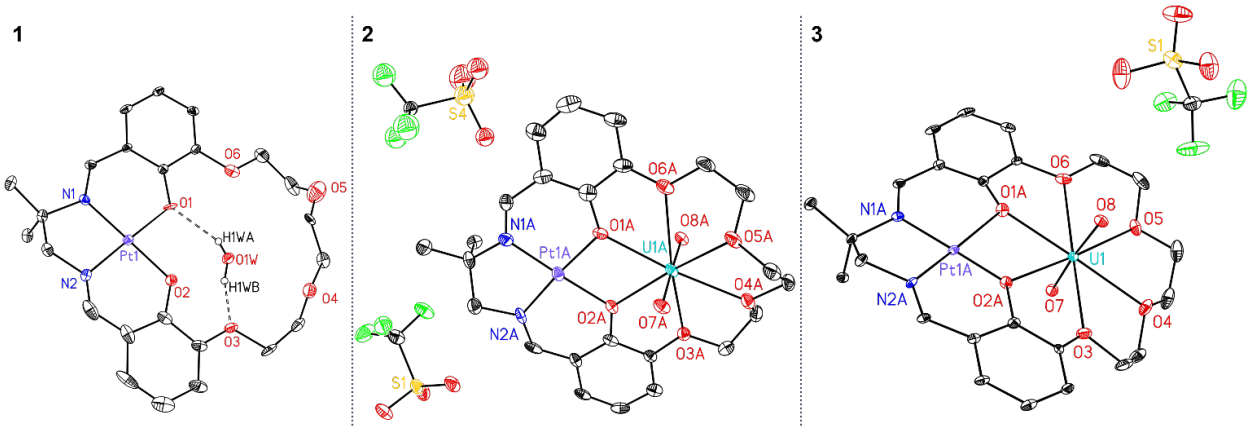

Figure 1. Solid-state structure (XRD) of **1**, **2**, and **3**. Two nearby triflate counter-anions from the asymmetric unit are shown here for **2**. All hydrogen atoms except for those associated with the co-crystallized water molecule, co-crystallized CH_3CN molecules, and minor components of disorder are omitted for clarity. Displacement ellipsoids are shown at 20% probability level.

https://doi.org/10.26434/chemrxiv-2023-qb7cc **ORCID:** https://orcid.org/0000-0003-4172-7460 Content not peer-reviewed by ChemRxiv. **License:** CC BY-NC-ND 4.0

Table 1. Comparison of selected structural parameters for **1**, **2**, and **3** from X-ray diffraction analysis.

	1	**2**	**3**
U–O_{oxo} (Å)[a]	-	1.751(9)[f]	1.819(4)
U–O_{phen} (Å)[a]	-	2.41(1)[f]	2.53(3)[e]
Pt–O_{phen} (Å)[a]	2.00(4)[e]	1.99(2)[f]	2.01(2)[e]
C–N_{imine} (Å)[a]	1.39(3)[e]	1.29(3)[f]	1.29(2)[e]
O1•••O2	2.74(5)[e]	2.59(2)[f]	2.64(4)[e]
Pt•••U (Å)	-	3.535(1)[f]	3.655(1)[e]
τ_4[b]	0.04(1)[e]	0.05(2)[f]	0.07(3)[e]
ω_{crown}[c]	0.20(1)[e]	0.23(3)[f]	0.12(2)[e]
Ψ_U[d]	-	0.05(1)	0.03(1)

[a]Defined as the average of the interatomic distances between the noted atom types. [b]Geometry index for four-coordinate complexes, with the values ranging from 1.00 to 0.00 for perfectly tetrahedral and square-planar geometries, respectively; see reference 25 for details. [c]Defined as root mean square deviation (RMSD) of O1–O6. [d]Defined as the absolute value of the distance between the uranium atom and the mean plane defined by O1–O6. [e]Values are reported as the mean of the relevant individual values corresponding to two disordered molecular orientations occupying the same site in the asymmetric unit. [f]Values were calculated as the mean of the relevant individual values corresponding to two independent molecules occupying distinct sites in the asymmetric unit. Stated e.s.d.'s on averaged distances were taken as the largest of the individual values in the refined data for the independent molecular species. Stated e.s.d's on the τ_4, ω_{crown}, and Ψ_U values were calculated as the standard deviation of the set of relevant values from the structural data. See Table S3 for details.

Contrasting with the profile measured for **1**, CV data for **2** exhibit a unique quasi-reversible redox process with $E_{1/2}$ = –0.18 V vs $Fc^{+/0}$ (see Figure 1 and Figure S44). Scan-rate-dependent data (50-300 mV/s; see Figure S45) confirmed the freely diffusional behavior of both the oxidized and reduced forms of the complex at the electrode, and we note that the peak-to-peak separation of the anodic and cathodic processes (ΔE_p) was 98 mV at 100 mV/s scan rate, indicative of rapid electron transfer behavior and fast interconversion of the oxidized and reduced forms of **2** at the electrode

https://doi.org/10.26434/chemrxiv-2023-qb7cc **ORCID:** https://orcid.org/0000-0003-4172-7460 Content not peer-reviewed by ChemRxiv. **License:** CC BY-NC-ND 4.0

surface.[26] As the ratio of the anodic to cathodic peak currents is near unity for all scan rates that we tested, we conclude that the reduction of **2** is chemically reversible (see Figure S46). As CV data for blank electrolyte and **1** lack any features resembling the wave measured for **2** at –0.18 V, this wave could be assigned as being $1e^-$ in nature and corresponding to generation of a complex, denoted **3**, that features uranium in the +5 oxidation state (for further characterization, *vide infra*). To the best of our knowledge, this redox chemistry represents the most positive reduction potential yet measured for U^{VI}/U^{V} redox cycling in a non-oxo-functionalized uranyl-derived species.[27] The dramatic shift in the U^{VI}/U^{V} couple that favors reduction can be attributed to the dicationic nature of the complex and stabilization of both U(VI) and U(V) species by crown ether coordination.

In order to understand these electrochemical findings and to validate the $1e^-$ nature of the reduction process at –0.18 V, we conducted chemical reduction experiments. We have found that decamethylferrocene, a mild, outer-sphere electron-transfer agent with $E_{1/2}$ = –0.48 V,[28] is sufficiently reducing to drive conversion of U(VI) to U(V), as demonstrated by titration of **2** with Cp^*_2Fe (see Figure 2b). The electronic spectrum of **2** in CH_3CN (0.1 mM) displays prominent features with $\lambda_{max} \approx$ 232, 259, and 331 nm, along with weaker absorbing features with $\lambda_{max} \approx$ 376 and 513 nm (see Figures S22 and S23). However, upon addition of 1 equiv. of Cp^*_2Fe, the spectral profile changes dramatically and isosbestically with U(V) and Fe(III) generation. The spectra confirm that conversion to the products is clean and complete, with isosbestic points at 426 and 630 nm; additionally, a feature at 784 nm can be confidently assigned as arising from a d-d transition associated with co-produced $Cp^*_2Fe^+$ (see Figures S24 and S26). Additions of Cp^*_2Fe beyond 1 equiv. led to no further significant spectral changes, in line with the CV data and the potentials accessible to Fe(II)-driven reduction. In accord with the measured $E_{1/2}(U^{VI}/U^{V})$ of –0.18

https://doi.org/10.26434/chemrxiv-2023-qb7cc **ORCID:** https://orcid.org/0000-0003-4172-7460 Content not peer-reviewed by ChemRxiv. **License:** CC BY-NC-ND 4.0

V, we have found that cobaltocene is also capable of generating **3**, consistent with its more negative $E_{1/2}$ value under our conditions of –1.33 V (see Figure S48).

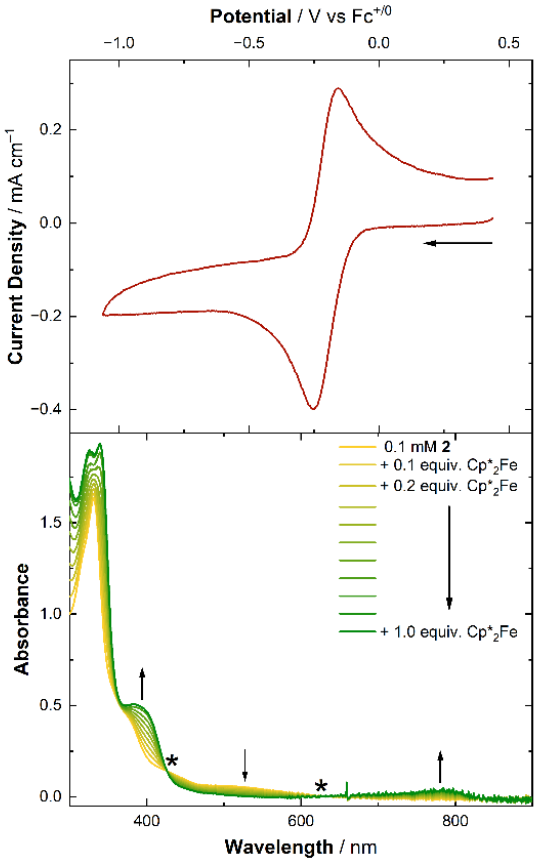

Figure 2. Top: Cyclic voltammogram of **2** in CH_3CN (0.1 M $[^nBu_4N]^+[PF_6]^-$, 100 mV/s) showing the U^{VI}/U^V redox couple. Bottom: Spectrochemical titration data for **2** with 1 equiv. of Cp^*_2Fe in CH_3CN. Isosbestic points are denoted by asterisk (*) and located at 426 and 630 nm.

To build up evidence that the observed reduction was uranium-centered, we collected near-infrared (NIR) spectra on *in situ* generated **3**. U(V) centers have been shown to exhibit sharp transitions in the NIR region with modest extinction coefficients (ε values) of ca. 10^2 M^{-1} cm^{-1}, providing a spectral signature for this oxidation state (O.S.).[29] **2** does not exhibit transitions in the NIR region, in line with the U(VI) O.S., but reduction of this complex by 1 equiv of either Cp^*_2Fe or Cp_2Co results in the appearance of two sharp features with λ_{max} = 1375 and 1410 nm (7272 and

https://doi.org/10.26434/chemrxiv-2023-qb7cc **ORCID:** https://orcid.org/0000-0003-4172-7460 Content not peer-reviewed by ChemRxiv. **License:** CC BY-NC-ND 4.0

7090 cm^{-1}) and ε values of 8.7 and 8.0 M^{-1} cm^{-1}, respectively (see Figure 3). These modest values are consistent with Laporte-forbidden 5*f*-to-5*f* transitions and resemble examples in the literature,[29] providing support for the generation of U(V).

Solution-state Raman spectroscopy was also conducted on **2** and *in situ* generated **3.** The Raman spectrum of **2** reveals the presence of the uranyl moiety, with a distinctive feature corresponding to the symmetric stretch (ν_{sym}) at 874 cm^{-1} (see Figure S41).[24] Upon reduction to form **3**, this feature was lost in accord with complete reduction of uranium. Spectra of **3** were checked for observation of ν_{sym} at lower wavenumber, but no features could be reliably attributed to U(V); the relevant spectral region from 870 to 700 cm^{-1}, however, displays a large feature associated with solvent that could mask signal(s) associated with reduced uranyl.

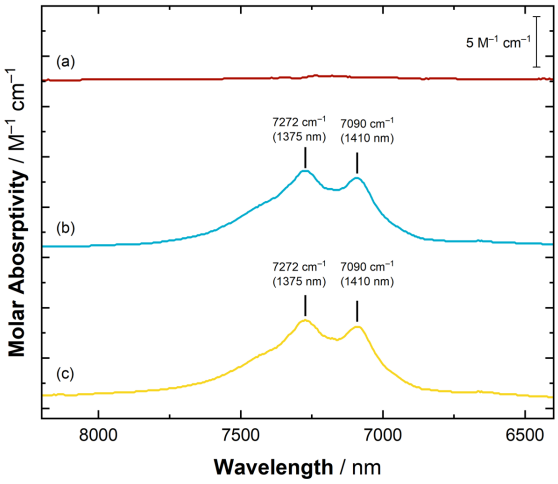

Figure 3. Near-IR data for **2** (spectrum a, red line), **3** generated by *in situ* reduction with Cp^*_2Fe (spectrum b, blue line), and **3** generated by *in situ* reduction with Cp_2Co (yellow line). Conditions: [U] = 10 mM in CH_3CN.

Encouraged by the spectroscopic results, we attempted chemical preparation and isolation of the $1e^-$ reduced complex **3** in CH_3CN. In order to achieve this, **2** was treated with 1 equiv. of Cp^*_2Fe in CH_3CN, resulting in an immediate color change of the solution from dark red to green.

https://doi.org/10.26434/chemrxiv-2023-qb7cc **ORCID:** https://orcid.org/0000-0003-4172-7460 Content not peer-reviewed by ChemRxiv. **License:** CC BY-NC-ND 4.0

The solvent was removed *in vacuo* to obtain a green powder which was found to contain a 1:1 mixture of **3** and $Cp^*_2Fe(OTf)$ (mixture denoted as **3a**). A similar procedure using Cp_2Co as reductant yielded a yellow-orange powder containing a 1:1 mixture of **3** and $Cp_2Co(OTf)$ (mixture denoted as **3b**). In line with the similar solubilities of **3** and the metallocene triflate salts, we found **3** challenging to isolate alone; the mixtures denoted **3a** and **3b** can be used for characterization or **3** can be separated and obtained in pure form by washing of **3b** with 1,2-dichloroethane. ^{1}H NMR spectra of **3a** and **3b** (d_3-CH_3CN) confirm formation of $Cp^*_2Fe^+$ and Cp_2Co^+, respectively; 10 new paramagnetically shifted resonances common to spectra of **3a** and **3b** were observed as well, consistent with clean, stoichiometric reduction of **2**. Elemental analysis (EA) confirmed the formulations of **3**, **3a**, **3b**, suggesting that the U(V) species is stable under inert atmosphere; this is in accord with its relatively positive reduction potential, which could engender stability during transport to the EA facility.

Crystals of **3** suitable for XRD analysis were grown by diffusion of Et_2O into a concentrated propionitrile solution containing the complex. In the structure that was obtained, the identities of the ligands in the first coordination sphere of uranium are identical to those found in the U(VI) analogue **2**, in accord with transfer of $1e^-$ to form **3** but no further chemical reactivity. The average $U–O_{oxo}$ bond distance is elongated to 1.819(4) Å; this elongation by 0.068 Å is consistent with U-centered reduction and formation of the U(V) oxidation state,[24] in line with the findings from NIR spectroscopy (Figure 3). The $U–O_{phenoxide}$ are elongated in **3**, consistent with generation of a more electron-rich uranium center upon reduction and attenuation of the effective Lewis acidity of this O.S. (Table 1). The $C–N_{imine}$ distances in **2** and **3** are indistinguishable, however, supporting localization of the added electron density on uranium and insignificant participation of the Pt site in the reduction process. The ω_{crown} parameter value of 0.120 in **3** is decreased from the value of

https://doi.org/10.26434/chemrxiv-2023-qb7cc **ORCID:** https://orcid.org/0000-0003-4172-7460 Content not peer-reviewed by ChemRxiv. **License:** CC BY-NC-ND 4.0

0.228 in **2**, suggesting that the less Lewis acidic U(V) oxidation state diminishes the out-of-place distortion of the crown-ether-like site; this finding is in accord with our prior studies of Lewis acidity-dependent crown behaviors in related Pd and Ni complexes.[18,19] On the basis of the Ψ_U values for **2** and **3**, U(V) can be concluded to sit more closely in the plane of the oxygen donor ligands than U(VI), suggesting an attractive supramolecular fit of $[U^VO_2]^+$ in the crown site.

Density functional theory (DFT) calculations were performed to probe the electronic structure of the crown-ligated uranium complexes prepared in this study, and to understand the measured weakening of the U–O_{oxo} interactions upon formation of the U(V) O.S. Starting with the coordinates of the structure of **2** from XRD, geometry optimizations were executed in the gas phase for the dicationic (**2**) and monocationic (**3**) species at the PBE0/ZORA-def2-SVP/SARC-ZORA-TZVP[30,31] level of theory. Based on these calculations, the asymmetric U–O_{oxo} stretching vibration of **2** was predicted to decrease by 114 cm^{-1} upon reduction, consistent with significant bond weakening. Experimental spectra were collected for both **2** and **3** in the solid state, and the relevant vibrations were found to shift by 137 cm^{-1} (see SI, pp. S28, S34, and S35), confirming that there is a significant weakening of the U–O_{oxo} bonding upon reduction despite the rather positive potential measured for U(V) generation in this system.

The calculations carried out for the U(VI) species **2** reveal a distinctly metal-centered LUMO bearing strong resemblance to the $f_{zx2\text{-}zy2}$ orbital, suggesting that the site of reduction in this complex would be centered primarily on uranium (see Figure 4). In line with this thesis, the HOMO of **3** is largely centered on the uranium center and strongly resembles a $f_{zx2\text{-}zy2}$ orbital, similar to the LUMO of **2**. The LUMO of **3**, however, is predominantly delocalized over the conjugated ligand backbone, in line with observation of a further irreversible reduction at –2.04 V for this species (see Figure S44).

https://doi.org/10.26434/chemrxiv-2023-qb7cc **ORCID:** https://orcid.org/0000-0003-4172-7460 Content not peer-reviewed by ChemRxiv. **License:** CC BY-NC-ND 4.0

NBO charge analysis[32,33,34] reveals a charge of +1.754 |e| at the U center in **2**; the charge at U decreases to +1.590 |e| in **3**, in line with generation of the U(V) formal oxidation state in this species (see Table S2). Furthermore, charge analysis indicates that there is buildup of negative charge on each of the oxo moieties (*yl* oxygens) by ca. –0.2 |e| per oxo upon U-centered reduction. This finding suggests that the *yl* moieties in **3** are more basic than in **2**[24] and could be more susceptible to reactivity with acidic reagents, a prospect currently under investigation.

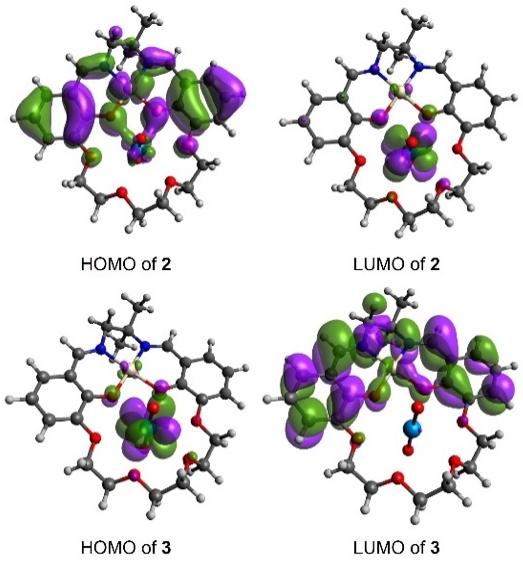

Figure 4. HOMO and LUMO of **2** (upper structures) and **3** (lower structures). The localization of the LUMO of **2** and the HOMO of **3** on the uranium metal center are consistent with generation of uranium(V) in **3**.

In conclusion, heterobimetallic complexes in which the uranyl ion is captured and coordinated in a crown ether coordination environment have been synthesized and fully characterized. The findings reported here suggest that crown-ether-type ligands could be quite useful for generation of uranium complexes with unique properties, particularly in terms of the positive reduction potentials engendered by formation of formally dicationic U(VI) complexes in this work. Despite the rarity of characterized uranyl-crown complexes to date, we have found that the crown ether

https://doi.org/10.26434/chemrxiv-2023-qb7cc **ORCID:** https://orcid.org/0000-0003-4172-7460 Content not peer-reviewed by ChemRxiv. **License:** CC BY-NC-ND 4.0

structure disfavors binding of exogeneous, anionic triflate ligands to the uranium center, despite its high Lewis acidity. A thorough experimental and theoretical exploration of the properties of uranium-crown complexes is now in progress in our laboratories.

Supporting Information

Structural data from X-ray diffraction analysis have been deposited in the Cambridge Structural Database under accession codes 2295456–2295458. Spectroscopic, electrochemical, and structural data are also given in the Supporting Information document, along with information on the computational methods and DFT-optimized Cartesian coordinates and computed energies. Cartesian coordinates for the experimental XRD structures and DFT-optimized structures have also been provided in XYZ-format files.

Acknowledgements

This work was supported by the U.S. Department of Energy, Office of Science, Office of Basic Energy Sciences through the Early Career Research Program (DE-SC0019169). A.C.E. was supported by a U.S. National Science Foundation Research Traineeship (NRT) at the University of Kansas (DGE-1922649). MZM and VAG were supported by ORNL's Laboratory Directed Research and Development (LDRD) program. This research used resources of the National Energy Research Scientific Computing Center (NERSC), a U.S. Department of Energy Office of Science User Facility located at Lawrence Berkeley National Laboratory, operated under Contract No. DE-AC02-05CH11231. Analytical data were obtained from the CENTC Elemental Analysis Facility at the University of Rochester, supported by the US National Science Foundation through award CHE-0650456.

Keywords: actinides • redox • electrochemistry • vibrational spectroscopy • near-infrared spectroscopy • density functional theory

https://doi.org/10.26434/chemrxiv-2023-qb7cc **ORCID:** https://orcid.org/0000-0003-4172-7460 Content not peer-reviewed by ChemRxiv. **License:** CC BY-NC-ND 4.0

References

[1] (a) C. J. Pedersen, *J. Am. Chem. Soc.* **1967**, *89*, 7017-7036. (b) M. R. Truter, Alkali Metal Complexes with Organic Ligands, *Structure and Bonding*, **1973**, *16*, 71-111. (c) M. E. Farago, *Inorg. Chim. Acta* **1977**, *25*, 71-76. (d) J. W. Steed, *Coord. Chem. Rev.* **2001**, *215*, 171-221.

[2] S. V. Nesterov, *Russ. Chem. Rev.* **2000**, *69*, 769-782.

[3] (a) M. G. Jalhoom, I. A. Mani, J. A. A. Juburi, *Radiochim. Acta.* **1985**, *38*, 215-218. (b) J. Shukla, R. Singh, A. Kumar, *Radiochim. Acta* **1991**, *54*, 73-78. (c) I. Billard, A. Ouadi, C. Gaillard, *Anal. Bioanal. Chem.* **2011**, *400*, 1555-1566.

[4] T. N. Poe, H. Ramanantoanina, J. M. Sperling, H. B. Wineinger, B. M. Rotermund, J. Brannon, Z. Bai, B. Scheibe, N. Beck, B. N. Long, S. Justiniano, T. E. Albrecht-Schönzart, C. Celis-Barros, *Nat. Chem.* **2023**.

[5] (a) A. Dejean, P. Charpin, G. Folcher, P. Rigny, A. Navaza, G. Tsoucaris, *Polyhedron* **1987**, *6*, 189-195. (b) T. Arliguie, L. Belkhiri, S.-E. Bouaoud, P. Thuéry, C. Villiers, A. Boucekkine, M. Ephritikhine, *Inorg. Chem.* **2009**, *48*, 221-230.

[6] K. Li, S. Hu, Q. Zou, Y. Zhang, H. Zhang, Y. Zhao, T. Zhou, Z. Chai, Y. Wang, *Inorg. Chem.* **2021**, *60*, 8984-8989.

[7] G. Folcher, P. Charpin, R.-M. Costes, N. Keller, G. C. de Villardi, *Inorg. Chim. Acta* **1979**, *34*, 87-90.

[8] A. Navaza, F. Villain, P. Charpin, *Polyhedron* **1984**, *3*, 143-149.

[9] L. Deshayes, N. Keller, M. Lance, A. Navaza, M. Nierlich, J. Vigner, *Polyhedron* **1994**, *13*, 1725-1733.

[10] M. Nierlich, J.-M. Sabattie, N. Keller, M. Lance, J.-D. Vigner, *Acta Crystallogr. C.* **1994**, *50*, 52-54.

[11] D. L. Clark, D. W. Keogh, P. D. Palmer, B. L. Scott, C. D. Tait, *Angew. Chem. Int. Ed.* **1998**, *37*, 164-166.

[12] M. Basile, E. Cole, T. Z. Forbes, *Inorg. Chem.* **2018**, *57*, 6016-6028.

[13] Y. Wang, S.-X. Hu, L. Cheng, C. Liang, X. Yin, H. Zhang, A. Li, D. Sheng, J. Diwu, X. Wang, *CCS Chem.* **2020**, *2*, 425-431.

[14] (a) P. Eller, R. Penneman, *Inorg. Chem.* **1976**, *15*, 2439-2442. (b) N. Armağan, *Acta Crystallogr. B.* **1977**, *33*, 2281-2284. (c) L. Deshayes, N. Keller, M. Lance, M. Nierlich, D. Vigner, *Acta Crystallogr. C.* **1993**, *49*, 16-19. (d) L. Deshayes, N. Keller, M. Lance, M. Nierlich, J.-D. Vigner, *Acta Crystallogr. C.* **1994**, *50*, 1541-1544.

[15] (a) M. M. Pyrch, J. M. Williams, T. Z. Forbes, *Chem. Commun.* **2019**, *55*, 9319-9322. (b) M. R. MacDonald, J. W. Ziller, W. J. Evans, *J. Am. Chem. Soc.* **2011**, *133*, 15914-15917.

[16] M. Keener, R. K. Shivaraam, T. Rajeshkumar, M. Tricoire, R. Scopelliti, I. Zivkovic, A.-S. Chauvin, L. Maron, M. Mazzanti, *J. Am. Chem. Soc.* **2023**, *145*, 16271-16283.

https://doi.org/10.26434/chemrxiv-2023-qb7cc **ORCID:** https://orcid.org/0000-0003-4172-7460 Content not peer-reviewed by ChemRxiv. **License:** CC BY-NC-ND 4.0

[17] (a) A. J. Ryan, J. W. Ziller, W. J. Evans, *Chem. Sci.* **2020**, *11*, 2006-2014. (b) D. N. Huh, J. W. Ziller, W. J. Evans, *Dalton Trans.* **2018**, *47*, 17285-17290. (c) M. Xémard, M. Cordier, F. Molton, C. Duboc, B. Le Guennic, O. Maury, O. Cador, G. Nocton, *Inorg. Chem.* **2019**, *58*, 2872-2880.

[18] A. Kumar, D. Lionetti, V. W. Day, J. D. Blakemore, *Chem. –Eur. J.* **2018**, *24*, 141-149.

[19] R. R. Golwankar, A. Kumar, V. W. Day, J. D. Blakemore, *Chem. –Eur. J.* **2022**, *28*, e202200344.

[20] S. R. Kelsey, A. Kumar, A. G. Oliver, V. W. Day, J. D. Blakemore, *ChemElectroChem* **2021**, *8*, 2792-2802.

[21] C. M. Dopp, R. R. Golwankar, S. R. Kelsey, J. T. Douglas, A. N. Erickson, A. G. Oliver, C. S. Day, V. W. Day, J. D. Blakemore, *Inorg. Chem.* **2023**, *62*, 9827-9843.

[22] J. C. Berthet, M. Lance, M. Nierlich, M. Ephritikhine, *Eur. J. Inorg. Chem.* **2000**, *2000*, 1969-1973.

[23] R. R. Golwankar, T. D. Curry, II, C. J. Paranjothi, J. D. Blakemore, *Inorg. Chem.* **2023**, *62*, 9765-9780.

[24] B. E. Cowie, J. M. Purkis, J. Austin, J. B. Love, P. L. Arnold, *Chem. Rev.* **2019**, *119*, 10595-10637.

[25] L. Yang, D. R. Powell, R. P. Houser, *DaltonTrans.* **2007**, 955–964.

[26] (a) P. Zanello, C. Nervi, F. F. De Biani, *Inorganic electrochemistry: theory, practice and application*, Royal Society of Chemistry, **2019**. (b) J.-M. Savéant, *Elements of Molecular and Biomolecular Electrochemistry*, Willey, New Jersey, **2019**.

[27] S. Fortier, T. W. Hayton, *Coord. Chem. Rev.* **2010**, *254*, 197-214.

[28] N. G. Connelly, W. E. Geiger, *Chem. Rev.* **1996**, *96*, 877-910.

[29] (a) D. D. Schnaars, G. Wu, T. W. Hayton, *Inorg. Chem.* **2011**, *50*, 4695-4697. (b) E. Pedrick, G. Wu, N. Kaltsoyannis, T. Hayton, *Chem. Sci.* **2014**, *5*, 3204-3213. (c) N. L. Bell, B. Shaw, P. L. Arnold, J. B. Love, *J. Am. Chem. Soc.* **2018**, *140*, 3378-3384. (d) K. Mizuoka, S. Tsushima, M. Hasegawa, T. Hoshi, Y. Ikeda, *Inorg. Chem.* **2005**, *44*, 6211-6218. (e) C. R. Graves, B. L. Scott, D. E. Morris, J. L. Kiplinger, *J. Am. Chem. Soc.* **2007**, *129*, 11914-11915.

[30] D. A. Pantazis, F. Neese, *J. Chem. Theory Comput.* **2011**, *7*, 677-684.

[31] F. Weigend, R. Ahlrichs, *Phys. Chem. Chem. Phys.* **2005**, *7*, 3297-3305.

[32] C. R. Landis, F. Weinhold, *The Chemical Bond: Fundamental Aspects of Chemical Bonding* **2014**, 91-120.

[33] E. D. Glendening, C. R. Landis, F. Weinhold, *Complementary Bonding Analysis* **2021**, 129-156.

[34] E. D. Glendening, J. K. Badenhoop, A. E. Reed, J. E. Carpenter, J. A. Bohmann, C. M. Morales, P. Karafiloglou, C. R. Landis, F. Weinhold, NBO 7.0, *Theoretical Chemistry Institute, University of Wisconsin, Madison WI*, **2018**.

https://doi.org/10.26434/chemrxiv-2023-qb7cc **ORCID:** https://orcid.org/0000-0003-4172-7460 Content not peer-reviewed by ChemRxiv. **License:** CC BY-NC-ND 4.0